Available online at www.sciencedirect.com
SCIENCE DIRECT®
Journal of Solid State Chemistry 179 (2006) 623–631
JOURNAL OF SOLID STATE CHEMISTRY
www.elsevier.com/locate/jssc

Neutron diffraction and magnetic study of the $Nd_{0.7}Pb_{0.3}Mn_{1-x}Fe_xO_3$ ($0 \leqslant x \leqslant 0.1$) perovskites

J.J. Blanco, M. Insausti, I. Gil de Muro, L. Lezama, T. Rojo*

Dpto. Química Inorgánica, Facultad de Ciencia y Tecnología. Universidad del País Vasco, U.P.V./E.H.U. Apdo. 644, E-48080 Bilbao, Spain

Received 27 July 2005; received in revised form 27 October 2005; accepted 13 November 2005
Available online 5 January 2006

Abstract

The effect of Fe doping on the ferromagnetic $Nd_{0.7}Pb_{0.3}Mn_{1-x}Fe_xO_3$ ($x = 0$, 0.025, 0.05, 0.075, 0.1) phases has been studied in order to analyze the double-exchange interaction. The structural and magnetic study has been carried out by neutron powder diffraction and susceptibility measurements between 1.7 and 300 K. The substitution of Fe at the Mn site results in reductions in both the Curie temperature T_c and the magnetic moment per Mn ion without appreciable differences in the crystal structures. All the compounds crystallize in *Pnma* space group. The thermal evolution of the lattice parameters of the $Nd_{0.7}Pb_{0.3}Mn_{1-x}Fe_xO_3$ ($x = 0.025$, 0.05, 0.075) compounds shows discontinuities in volume and lattice parameters close to the magnetic transition temperature. Increasing amounts of Fe^{3+} reduces the double exchange interactions and no magnetic contribution for $x = 0.1$ is observed. The magnetic structures of $Nd_{0.7}Pb_{0.3}Mn_{1-x}Fe_xO_3$ ($x = 0$, 0.025, 0.05, 0.075) compounds show that the Nd and Mn ions are ferromagnetically ordered.

Keywords: Fe-doped manganites; Magnetism; Crystal structure; Neutron diffraction; Perovskites

1. Introduction

The hole-doped perovskites such as $Ln_{1-x}A_xMnO_3$ (Ln = La, Nd, Pr; A = Ca, Sr, Ba, Pb) have attracted considerable attention these last years owing to their 'colossal' magnetoresistance (CMR) effect near the paramagnetic (PM) to ferromagnetic (FM) transition temperature, T_c [1–3]. The substitution of a divalent alkaline element by Ln^{3+} leads to FM Mn^{4+}–Mn^{3+} double exchange (DE) interactions competing with antiferromagnetic (AF) Mn^{3+}–Mn^{3+} superexchange interactions. Nevertheless, in order to understand the electronic and magnetic properties, some other effects should be taken into account: lattice effects and polaron formation [4], magnetic frustration [5,6], charge ordering in half-doped manganites and phase separation effects [7,8].

In the perovskite manganese oxide, the introduction of other transition metal elements, which exhibit the dissimilar electronic configuration to the Mn site, should lead to dramatic effects associated with the electronic configuration mismatch between Mn and the other substituted magnetic ions. The *B*-site doping directly reduces the content of mobile e_g electrons when Mn^{3+} is replaced. Considering that e_g electrons would tend to distort its local lattice, forming a Jahn–Teller polaron, the Mn^{3+} substitution should induce changes in the electronic structure. In this sense, and in order to avoid the lattice distortion, the Fe atom has been selected regarding the identical ionic radii of Fe^{3+} and Mn^{3+} [9]. Thus, the number of Mn^{3+}/Mn^{4+} pairs is reduced, which is an essential ingredient for the DE interaction.

Most of the studies on the Fe-doped substituted manganites have been focused on $La_{0.7}Ca_{0.3}Mn_{1-x}Fe_xO_3$ [10–13], $La_{0.7}Sr_{0.3}Mn_{1-x}Fe_xO_3$ [14] and $La_{0.7}Pb_{0.3}Mn_{1-x}M_xO_3$ [15,16] systems. Strontium-substituted neodymium single crystals have been recently studied [17,18]. Although no apparent structural changes were associated with Fe doping, both ferromagnetism and metallic conduction were systematically reduced. It has been found that with the same amount of Fe doping, the Curie temperature T_c decreases faster in the Nd-based system than in the

*Corresponding author. Fax: +34 94 6013500.
E-mail address: qiproapt@lg.ehu.es (T. Rojo).

0022-4596/$ - see front matter © 2005 Elsevier Inc. All rights reserved.
doi:10.1016/j.jssc.2005.11.017

corresponding La-based system. At high Fe-doping levels ($x > 0.1$), the strong competition between the Mn–O–Mn DE and the Mn–O–Fe superexchange interactions might also result in spin-glass behavior [19,20].

Although the properties of lanthanum manganites have been well studied, here we focus the study on the variation of the crystallographic structure and the magnetic behavior of different Fe doped $Nd_{0.7}Pb_{0.3}Mn_{1-x}Fe_xO_3$ ($x = 0$, 0.025, 0.05, 0.075, 0.1) compositions. The investigations have been performed in a small range of iron composition in order to know the quantity necessary to eliminate the DE interaction and to obtain additional information concerning microscopic lattice disorder, which has strong influence on the magnetic properties. Neutron diffraction techniques have been used to elucidate the influence of iron doping and the effect of neodymium on the crystal and magnetic structures.

2. Experimental section

2.1. Syntheses

The polycrystalline $Nd_{0.7}Pb_{0.3}Mn_{1-x}Fe_xO_3$ ($x = 0$, 0.025, 0.05, 0.075, 0.1) compounds were prepared by thermal decomposition from the precursor complexes, using citric acid as a complexing agent. To an aqueous solution containing high purity Nd_2O_3, $Pb(NO_3)_2$, $Mn(C_2H_3O_2)_2 \cdot 9H_2O$ and FeO in stoichiometric proportion, citric acid was added. The molar ratio of total metal ions to citric acid was 1:3. After stirring for 1 h, ethylenglycol was added (3/4 mol of ethylene per 1 mol of citric acid). The solution was dehydrated at 373 K in a sand bath into a gel, which was slowly incinerated in a crucible for 1 day at 723 K in air. Then, they were fired at 973 K for 10 h. The microcrystalline powder obtained was pelletized and sintered at 1073 K for 12 h in flowing oxygen. Inductively coupled plasma atomic emission spectroscopy (ICP-AES) analysis showed the expected stoichiometry for Nd, Pb, Mn and Fe in all samples. The microstructure of the obtained particles, observed by scanning electron microscopy, reveals uniform and fine grain growth, around 0.3–0.5 μm. The image of one of the samples can be visualized in Fig. 1. Particle sizes have been measured by low angle laser light scattering (LALLS) (Supplemental Materials). The sol–gel process used in the synthesis of the compounds gives rise to the formation of small size particles with a considerable degree of agglomeration, which can be attributed to the fineness of the grains.

2.2. Experimental techniques

The first crystallographic characterization of the samples was performed by X-ray powder diffraction analysis at room temperature using a Stoe/Stadi-P diffractometer equipped with a Ge(III) monochromator, working with Cu$K\alpha_1$ radiation, over the interval $10^\circ \leqslant 2\theta \leqslant 80^\circ$ in increments of 0.02° (2θ). The diffraction maxima of the phases were indexed in the orthorhombic space group *Pnma*.

Neutron diffraction data were performed at the high-flux reactor at the Institute Laue Langevin (ILL) in Grenoble. Three different instruments were used. For accurate refinements of the nuclear and magnetic structures, measurements were carried out on D2B, using a wavelength $\lambda = 1.594$ Å. Measurements of the temperature dependence of the structural and magnetic properties were carried out on D1B and D20 instruments, using wavelengths of $\lambda = 2.5210$Å and 2.41 Å, respectively. The diffraction spectra were registered in the angular range $5 \leqslant 2\theta \leqslant 100^\circ$, in steps of 0.05° in the 1.7–300 K temperature range. Data were Rietveld [21] fitted using the FullProf program [22]. A Pseudo-Voigt function was used to model the peaks, with the asymmetry correction proposed by Baldinozzi et al. [23]. In all the cases, the background was

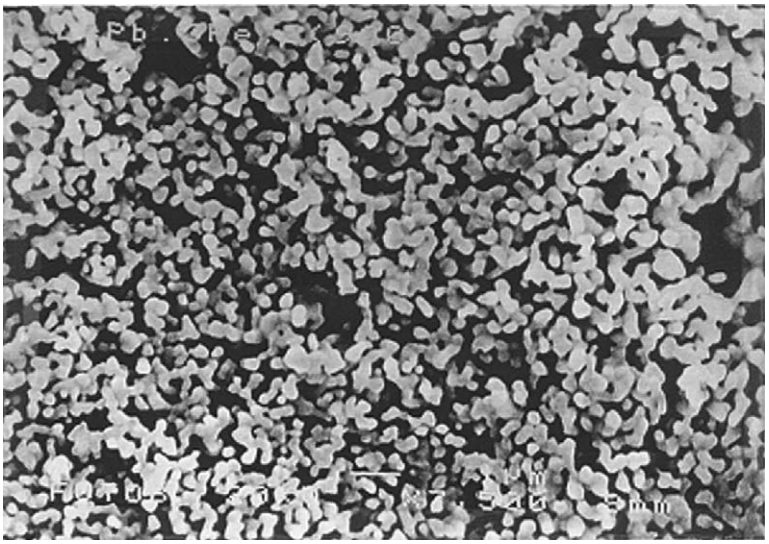

Fig. 1. SEM photograph of the $Nd_{0.7}Pb_{0.3}Mn_{0.9}Fe_{0.1}O_3$ phase sinterized at 900 °C.

fitted by linear interpolation between regions where no Bragg peaks appear. The coherent neutron scattering lengths for Nd, Pb, Mn, Fe and O were 7.69, 9.405, −3.73, 9.45 and 5.803 fm, respectively. In the final run, the following parameters were refined: unit-cell parameters, zero-point, half-width, pseudo-Voigt, asymmetry parameters, scale factor, atomic coordinates and thermal isotropic factors.

Susceptibility measurements were performed in the temperature range 1.8–300 K using a QUANTUM DESIGN MPMS-7 SQUID magnetometer at magnetic fields between 0 and 7 T. The zero-field cooling (ZFC) and field cooling (FC) curves were performed under an applied magnetic field of 10 mT. $M(T)$ curves at 1 T applied field and hysteresis loops at 10 K and up to 7 T were also obtained.

3. Results and discussion

3.1. Structural characterization

The structural characterization of the $Nd_{0.7}Pb_{0.3}Mn_{1-x}Fe_xO_3$ phases has been carried out in both PM and FM regions. The phases have been measured on D2B and D1B instruments. D2B was used at 190 and 10 K for $x = 0$ and at 250, 110, 50, 10 and 1.5 K for $x = 0.1$. The $x = 0.025$, 0.05 and 0.075 phases were measured on D1B between 4 and 200 K. Weak extra lines corresponding to a small amount of Mn_2O_3 (<3%, Bixbyite ASTM No. 41-1442) appear due to the difficulty in the attainment of high amounts of samples. Neutron diffraction measurements showed all samples to have O″-orthorhombic symmetry with $b/\sqrt{2} < a < c$ distortion in the studied temperature range. The refinements performed show Nd/Pb atoms at 4*c* position, Mn/Fe at 4*b*, O1 at 4*c* and O2 at 8*d* crystallographic positions. The mentioned atomic disposition yields two Mn–O(1)–Mn and four Mn–O(2)–Mn equivalent angles. The results obtained from the refinement, above T_c and at low temperatures, are listed in Tables 1 and 2.

The unit cell volume and the Mn/Fe–O distances slightly increase with increasing the Fe content. These features indicate that the distortion is nearly independent of the x value, in good agreement with the similar sizes of the Fe^{3+} and Mn^{3+} ions. It is to note the thermal evolution of the unit cell parameters when cooling down to low temperatures. A unit cell contraction is observed. This fact is related to the existence of shorter Mn–O distances at lower

Table 1
Selected parameters refined from D2B neutron diffraction data for (a) $Nd_{0.7}Pb_{0.3}MnO_3$ and (b) $Nd_{0.7}Pb_{0.3}Mn_{0.9}Fe_{0.1}O_3$. Nd/Pb are at 4*c* positions (*x*, 1/4, *z*); Mn/Fe at 4*b* (0, 0, 1/2), O(1) at 4*c* (*x*, 1/4, *z*) and O(2) at 8*d* (*x*, *y*, *z*)

S.G	*a* (190 K) *Pnma*	*a* (10 K) *Pnma*	*b* (250 K) *Pnma*	*b* (1.5 K) *Pnma*
a (Å)	5.4584(1)	5.4497(4)	5.4597(4)	5.459(1)
$b/\sqrt{2}$(Å)	5.4577(2)	5.4483(5)	5.4583(6)	5.459(1)
c (Å)	5.4837(1)	5.4737(5)	5.4864(4)	5.479(2)
V (Å^3)	231.02(1)	229.84(3)	231.22(3)	231.03(9)
μ_{Mn} (μ_B)	0	2.89(2)	0	1.50(7)
Nd/Pb				
x	0.0165(3)	0.0157(7)	0.0106(9)	0.023(1)
z	−0.0028(4)	−0.0031(8)	−0.0004(9)	−0.001(2)
Biso (Å^2)	0.57(2)	0.56(4)	0.59(4)	0.3(1)
Mn/Fe *Biso* (Å^2)	0.45(3)	0.7(1)	1.44(3)	0.8(3)
O(1)				
x	0.4923(6)	0.489(1)	0.484(2)	0.497(1)
z	0.0633(4)	0.069(1)	0.0619(9)	0.067(3)
Biso (Å^2)	1.16(4)	1.4(1)	1.4(1)	0.8(3)
O(2)				
x	0.2737(4)	0.2742(6)	0.2704(8)	0.276(1)
y	0.0334(2)	0.0310(5)	0.0316(4)	0.033(1)
z	0.7273(4)	0.7262(6)	0.7310(9)	0.726(1)
Biso (Å^2)	1.48(3)	1.12(9)	1.38(7)	0.9(2)
R_{wp} (%)	4.10	3.86	6.38	7.58
R_p (%)	3.22	2.97	4.99	5.91
R_{mag} (%)		3.08		
χ^2	1.61	2.05	1.40	1.24
Mn–O(1)	1.9610(4) (× 2)	1.964(1) (× 2)	1.961(1) (× 2)	1.965(2) (× 2)
Mn–O(2)	1.963(2) (× 2)	1.955(3) (× 2)	1.961(5) (× 2)	1.969(7) (× 2)
	1.956(2) (× 2)	1.954(3) (× 2)	1.952(5) (× 2)	1.954(3) (× 2)
⟨Mn–O⟩	1.960(2)	1.958(2)		1.958(3)
Mn–O(1)–Mn	159.47(2) (× 2)	157.44(5) (× 2)	159.37(5) (× 2)	158.4(1) (× 2)
Mn–O(2)–Mn	161.55(1) (× 4)	162.18(1) (× 4)	163.07(2) (× 4)	161.0(3) (× 4)
⟨Mn–O–Mn⟩	160.86(1)	160.60(2)	161.84(3)	160.13(3)

Table 2
Selected parameters refined from D1B neutron diffraction data for $Nd_{0.7}Pb_{0.3}Mn_{1-x}Fe_xO_3$ ($x = 0.025, 0.05, 0.075$): (a) at 4 K and (b) 185 K* and 200 K**

(a)	$NdPbMnFe_{0.025}$	$NdPbMnFe_{0.05}$	$NdPbMnFe_{0.075}$
T (K)	4	4	4
a (Å)	5.465(4)	5.466(3)	5.469(5)
$b/\sqrt{2}$ (Å)	5.458(2)	5.461(1)	5.463(2)
c (Å)	5.475(1)	5.478(1)	5.479(2)
V (Å^3)	231.1(2)	231.2(1)	231.5(2)
R_p (%)	1.86	1.89	2.32
R_{wp} (%)	2.48	2.48	3.03
χ^2	6.26	6.30	4.28
(b)	$NdPbMnFe_{0.025}$	$NdPbMnFe_{0.05}$	$NdPbMnFe_{0.075}$
T (K)	185	185	200
a (Å)	5.462(1)	5.463(1)	5.464(1)
$b/\sqrt{2}$ (Å)	5.459(2)	5.460(3)	5.464(3)
c (Å)	5.490(1)	5.492(2)	5.486(2)
V (Å^3)	231.5(1)	231.7(1)	231.7(1)
R_p (%)	1.89	2.04	2.24
R_{wp} (%)	2.60	2.69	2.92
χ^2	6.72	7.73	4.06

temperatures, which range from 1.9580(3)Å at 250 K to 1.9566(3)Å at 10 K for the $Nd_{0.7}Pb_{0.3}Mn_{0.9}Fe_{0.1}O_3$ phase. The thermal evolution of the lattice parameters for the $Nd_{0.7}Pb_{0.3}Mn_{1-x}Fe_xO_3$ ($x = 0.025$, 0.05, 0.075) compounds obtained from D1B data is shown in Fig. 2. A greater decrease of the c parameter can be observed, confirming the major influence of this parameter to the octahedral distortion. The discontinuities in volume and lattice parameters close to the magnetic transition temperature, which clearly appear for $x = 0.025$ and 0.075 phases, could be related to the alterations produced by the energy associated to the magnetic transition.

The Mn–O(2)–Mn angles, related to the buckling of the equatorial planes, are smaller (159.47(2)° for $Nd_{0.7}Pb_{0.3}MnO_3$) than the Mn–O(1)–Mn ones (161.55(1)°) indicating tilting of octahedra along the b-axis. The values are in good accordance with those observed in other manganites with a similar average A cationic radius, $\langle r_A \rangle = 1.22$ Å. The MnO_6 octahedra show smaller distortions when increasing $\langle r_A \rangle$ [24,25].

3.2. Magnetic properties

The temperature dependence of the FC and ZFC magnetizations for all the phases has been performed and represented in Fig. 3. Some results concerning the $x = 0$ and 0.1 compositions have been previously reported by the authors [26]. Characteristic magnetic data are given in Table 3. The usual ferro to PM transition appears at different temperatures depending on the iron amounts. The T_c values have been obtained as the minimum of the curve dM/dT calculated from the ZFC curves. The T_c in the parent compound, $Nd_{0.7}Pb_{0.3}MnO_3$, is 175 K and gradually decreases to lower temperatures when the content of Fe increases. In these phases, 1% Fe doping causes a decrease in T_c by approximately 10 K, similar to that observed in other compounds such as $La_{0.7}Sr_{0.3}MnO_3$ or $La_{0.7}Pb_{0.3}MnO_3$ [15,27] and quite different from the obtained for the $Nd_{0.67}Sr_{0.33}Mn_{1-x}Fe_xO_3$ system, where a drop of 18 K per 1% Fe was observed [17,28]. The Fe amounts are more effective in weakening DE when the bandwidth of e_g electrons narrows. This narrowing is more significant for the Nd/Sr phases than for Nd/Pb ones, probably due to the presence of lead, which increases the ionic radius at A site.

Another interesting effect of the Fe substitutions on the ZFC curves can be observed in Fig. 3. In this way, at temperatures just below T_c, the magnetization reaches the maximum value and decreases until practically zero. This effect is more significant with higher iron amounts. In this case, the DE Mn–O–Mn mechanism competes with the superexchange Mn–O–Fe interactions and consequently the ZFC-FC curves display irreversibility and λ-shape traces, indicating the existence of a short-range spin ordering [29]. The values of the effective magnetic moments, μ_{eff}, determined from the χT curves at 300 K, are higher than those expected for a PM behavior, which is around 5.64 B.M (see Table 3). This result is in good agreement with the existence of short range FM interactions up to room temperature, as was observed from EPR measurements [26].

The magnetization measurements as a function of the magnetic field at 10 K have been represented in Fig. 4. An FM behavior is observed for all phases with a decrease of the magnetization when increasing the iron content. The highest value of magnetization at 7 T corresponds to $Nd_{0.7}Pb_{0.3}MnO_3$ ($M/N\beta \approx 3.31$ per Mn site) (see Table 3). This value is slightly lower than the corresponding to a free ion with 70% Mn^{3+} and 30% Mn^{4+} ($M/N\beta \approx 3.7$), as was observed in related manganites [15,16]. The low field

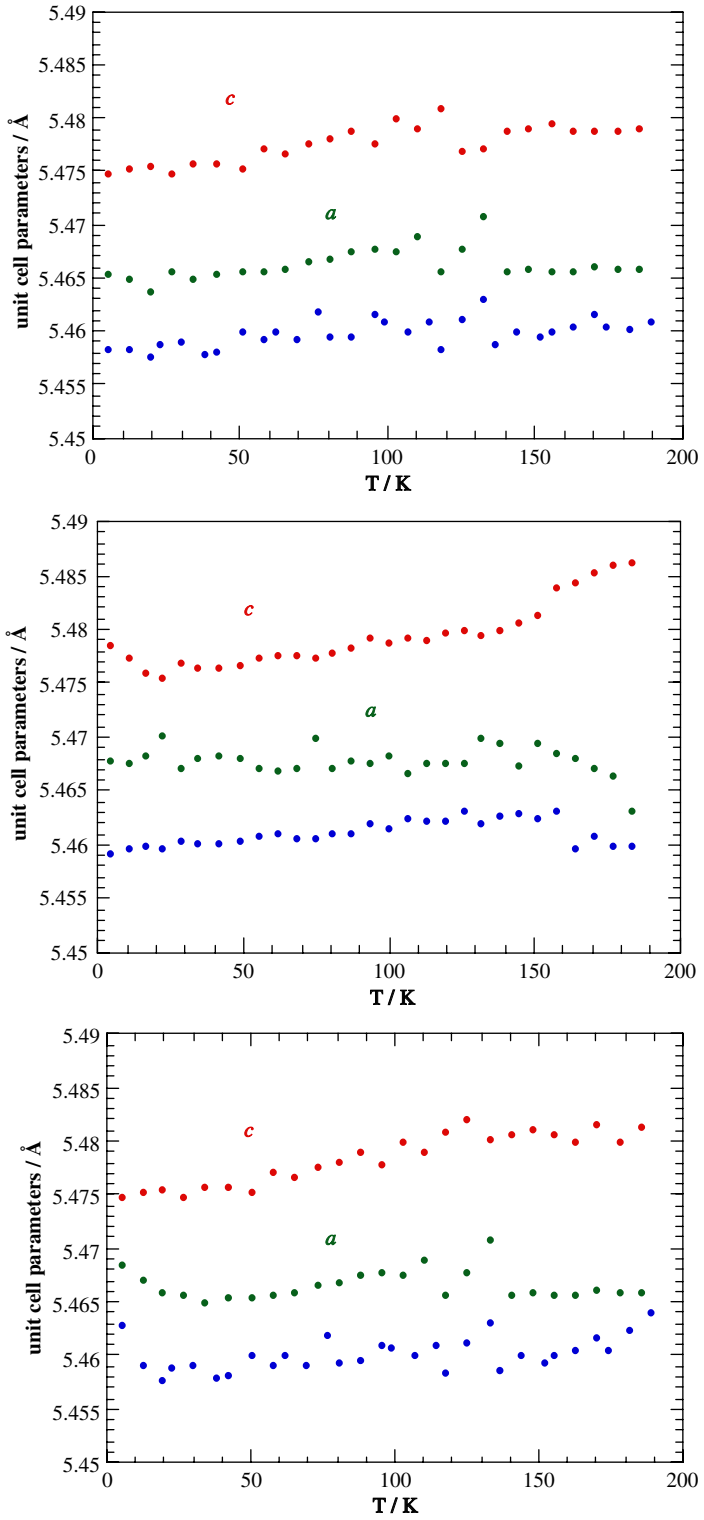

Fig. 2. Thermal evolution of the lattice parameters for the phases: (a) $NdPbMnFe_{0.025}$, (upper), (b) $NdPbMnFe_{0.05}$ (medium) and (c) $NdPbMnFe_{0.075}$ (lower).

magnetization data over ± 5 kOe show the presence of hysteresis with low coercitive fields, between 211 and 520 Oe, and remanent values around 2000 emu/mol, which are characteristic of these kinds of systems [30]. The increase of iron content gives rise to an antiferromagnetic coupling between Mn and Fe ions and the DE is progressively suppressed, weakening both the FM and metallic behaviors of the samples [17,18,31].

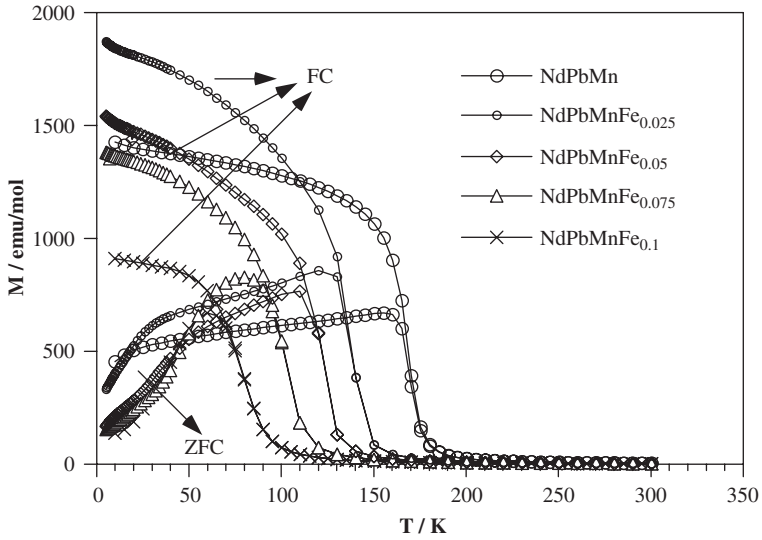

Fig. 3. Thermal evolution of the magnetization (field cooling, FC and zero field cooling, ZFC) for the $Nd_{0.7}Pb_{0.3}Mn_{1-x}Fe_xO_3$ ($x = 0$, 0.025, 0.5, 0.075, 0.1) phases under an applied magnetic field of 10 mT.

Table 3
Magnetic values for the $Nd_{0.7}Pb_{0.3}Mn_{1-x}Fe_xO_3$ phases: (a) T_c calculated from the minimum of the dM_{FC}/dT curve, (b) μ_{eff} determined from the χT curves at 300 K, (c) values calculated from hysteresis loops at 10 K and 7 T, (d) $M/N\beta$ electrons for magnetic atom, (e) H_c values in O_e and (f) M_r values in emu/mol

	T_c (K)[(a)]	μ_{eff} [(b)]	$M/N\beta$[(d),(c)]	H_c[(c),(e)]	M_r[(c),(f)]
NdPbMn	175	11.06	3.31	394	2727
$NdPbMnFe_{0.025}$	144	9.41	3.29	246	2261
$NdPbMnFe_{0.05}$	130	8.74	3.02	211	1658
$NdPbMnFe_{0.075}$	107	8.82	2.89	316	1957
$NdPbMnFe_{0.1}$	75	8.14	2.22	527	1989

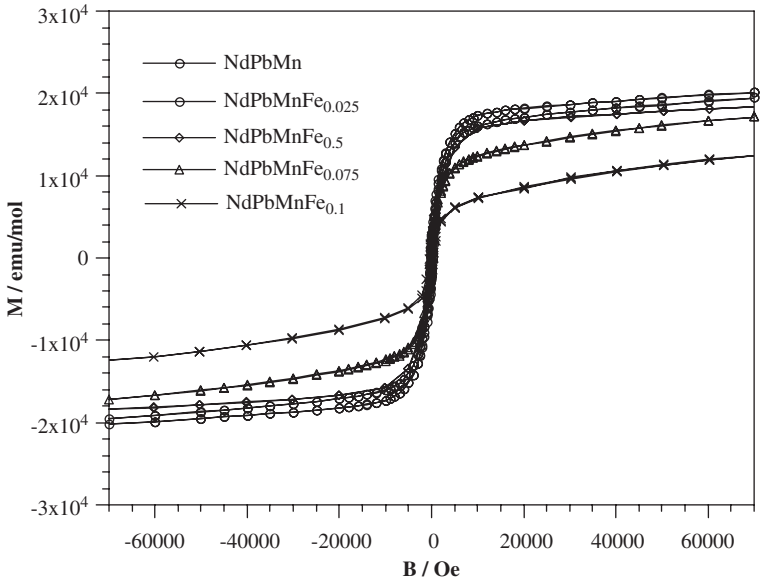

Fig. 4. Hysteresis loops at 10 K for the $Nd_{0.7}Pb_{0.3}Mn_{1-x}Fe_xO_3$ ($x = 0$, 0.025, 0.5, 0.075, 0.1) phases.

3.3. Magnetic structure

NPD data for $Nd_{0.7}Pb_{0.3}MnO_3$ were collected on D2B at 190 and 10 K. At low temperatures, a strong magnetic contribution appears at (002), (121) and (200) Bragg positions. Extra Bragg intensity to the nuclear peaks is observed in (101), (020), (220) and (022) positions, corresponding to the magnetic alignment of the Mn

moments. The Rietveld refinement of data was performed using a simple FM model with both Mn and Nd magnetic moments aligned along one crystallographic axis. The saturated magnetic moments reach values of 2.89(2) μ_B and 0.19(2) μ_B for Mn and Nd, respectively, being similar to those obtained in other neodymium systems where parallel ordering was considered [32]. The total contribution to the magnetic moment is in good agreement with 3.31*e*—calculated from the hysteresis loops.

In order to study the evolution of the magnetic peaks with temperature for all the samples, diffraction patterns were recorded on D20 for $x = 0$, 0.1 and on D1B for $x = 0.025$, 0.5 and 0.75 phases in the 4–200 K temperature range. A progressively decrease in the intensity of the

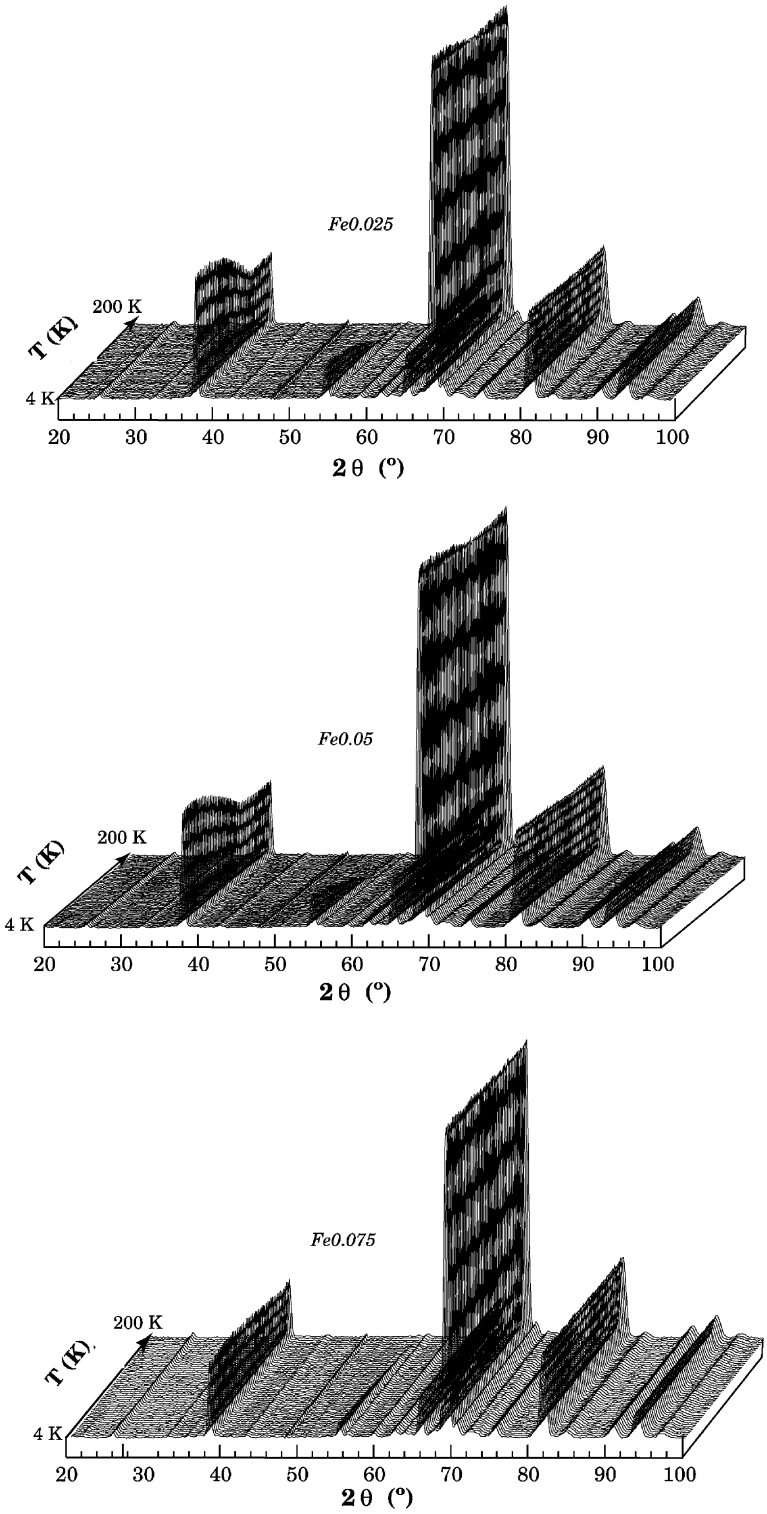

Fig. 5. Thermal evolution of neutron diffraction patterns for the $Nd_{0.7}Pb_{0.3}Mn_{1-x}Fe_xO_3$ ($x = 0.025$, 0.5, 0.075) phases measured at D1B.

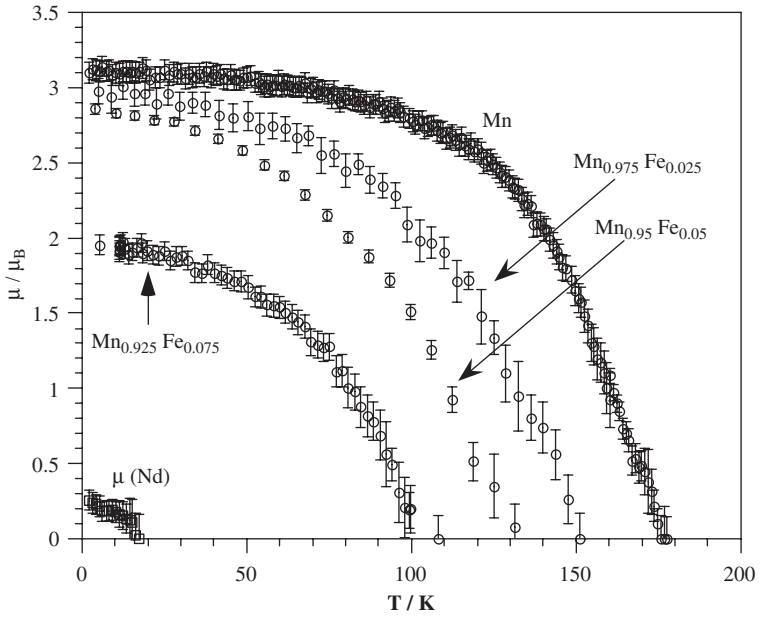

Fig. 6. Evolution of the Mn magnetic moments with temperature for the $Nd_{0.7}Pb_{0.3}Mn_{1-x}Fe_xO_3$ ($x = 0$, 0.025, 0.5, 0.075) phases and evolution of Nd moment for $Nd_{0.7}Pb_{0.3}MnO_3$.

magnetic peaks is observed when increasing the Fe content giving rise to a magnetic frustration (Fig. 5). When the concentration of Fe reaches 10%, the pattern does not show any magnetic contribution, because of an absence of the magnetic ordering in this temperature range. Sequential refinements of data for the $Nd_{0.7}Pb_{0.3}Mn_{1-x}Fe_xO_3$ phases ($x = 0$, 0.025, 0.05 and 0.075) were performed with Mn and Nd moments along the *c*-axis, using FULLPROF program. The evolution of the manganese magnetic moments with temperature (Fig. 6) shows the characteristics of the FM–PM transitions as was observed from magnetic measurements. The manganese magnetic moment reaches the maximum value of $3.10\,\mu_B$ for the $Nd_{0.7}Pb_{0.3}MnO_3$ phase and progressively decreases until $1.95\,\mu_B$ when the content of iron is 7.5%. The Nd moments only appear for the $Nd_{0.7}Pb_{0.3}MnO_3$ phase where the maximum value is $0.3\,\mu_B$. This value decreases down to $0\,\mu_B$ at approximately 15 K where the neodymium contribution disappears [33].

In order to improve the knowledge of the magnetic behavior for the $Nd_{0.7}Pb_{0.3}Mn_{0.9}Fe_{0.1}O_3$ phase, neutron measurements on D2B instrument at 250, 110, 50, 10 and 1.5 K and different magnetic fields between 0.01 and 5 T were performed. Magnetic contribution without magnetic field is only observed at temperatures near 2 K. At this temperature, a value of $1.50(7)\,\mu_B$ was obtained for the manganese moment ($x = 0.1$), which is slightly lower to that observed for the $x = 0.075$ composition ($1.95\,\mu_B$) as the increase in iron content reduces the DE coupling. When applying a magnetic field at low temperatures (1.5 K), the intensity of the 1 0 1 and 0 2 0 reflections increases and diffraction maxima corresponding to 0 0 2, 1 2 1 and 2 0 0 reflections appear, due to the alignment of the Mn and Nd spins. The magnetic structures were indexed using the magnetic model previously described. The values of the refined parameters are shown in Table 4. The variation of the magnetic field has not any influence on the cell parameters, but an increase of the magnetic moment for both manganese and neodymium ions is observed. This fact can be explained by the decrease of the antiferromagnetic interactions and the increase of the FM ones, the total magnetic moment being lower than the theoretical one.

Table 4
Selected parameters refined from D2B neutron diffraction data for $Nd_{0.7}Pb_{0.3}Mn_{0.9}Fe_{0.1}O_3$ at different magnetic fields at 1.5 K

H (T)	0.01	1	2	5
S.G.	*Pnma*	*Pnma*	*Pnma*	*Pnma*
a (Å)	5.459(1)	5.4597(9)	5.4550(2)	5.4546(2)
$b/\sqrt{2}$ (Å)	5.459(1)	5.4610(1)	5.4538(4)	5.4533(3)
c (Å)	5.479(2)	5.481(1)	5.4792(2)	5.4785(2)
V (Å^3)	231.03(9)	231.12(7)	230.53(3)	230.47(1)
μ_{Mn} (μ_B)	1.49(7)	2.09(4)	2.16(5)	2.60(5)
μ_{Nd} (μ_B)	0	0.12(4)	0.40(4)	0.74(4)
R_{wp} (%)	7.58	4.51	4.00	3.58
R_p(%)	5.91	3.55	3.13	2.80
χ^2	1.24	1.37	1.63	1.81

4. Conclusion

The sol–gel method has been used to synthesize $Nd_{0.7}Pb_{0.3}Mn_{1-x}Fe_xO_3$ ($x = 0$, 0.025, 0.05, 0.075, 0.1) homogeneous oxides with small grain size. Rietveld analysis of the neutron diffraction data shows orthorhombic symmetry with $b/\sqrt{2} < a < c$ distortion in the studied temperature range. The increase of Fe amounts does not affect considerably the unit cell volume and Mn/Fe–O distances. In these materials, local strain effects induced by

the dopant amount are not dominant in controlling the magnetotransport properties and the lattice effect can be considered as negligible due to the similar radius of Fe and Mn. When cooling down to low temperatures, thermal evolution of the unit cell parameters related to shorter Mn–O distances can be observed. However, Mn-site doping causes a direct effect on the magnetic properties as DE mechanism is directly affected. A systematic study of the magnetic properties in the compounds shows that 1% Fe doping produces a decrease in the T_c about 10 K. This effect is similar to that observed by other authors in $La_{0.7}Sr_{0.3}MnO_3$ or $La_{0.7}Pb_{0.3}MnO_3$ compounds [15,16,27] and can be explained by a general weakening of the FM DE interactions and an increase in the contribution of the AFM ones arising from superexchange. The observed irreversibility between the ZFC and FC magnetization curves could be explained as due to the presence of a spin-glass phase transition from kinetic freezing of magnetic domains.

The magnetic structure of the $Nd_{0.7}Pb_{0.3}Mn_{1-x}Fe_xO_3$ ($x = 0$, 0.025, 0.05, 0.075) phases indicates that both types of ions, Nd and/or Mn are ferromagnetically ordered. The neutron diffraction study for $Nd_{0.7}Pb_{0.3}Mn_{0.9}Fe_{0.1}O_3$ does not show any FM Bragg contribution or extra peaks until 2 K. When increasing the magnetic field a magnetic contribution appears. A competition between FM and antiferromagnetic interactions together with the random substitution of Fe ions in B places gives rise to a randomly FM canted phase with low net moments.

Acknowledgments

This work has been carried out with the financial support of the Ministerio de Educación y Ciencia (MAT2004-02425) and University of the Basque Country (UPV, 9/UPV 00169.310-13494/2001) which we gratefully acknowledge. The authors would also like to thank Dr. Teresa Fernández from the ILL for help in collecting diffraction data and the ILL for the provision of beamtime.

Appendix A. Supplementary materials

Supplementary data associated with this article can be found in the online version at doi:10.1016/j.jssc.2005.11.017.

References

[1] R.M. Kusters, J. Singleton, D.A. Keen, R. McGreevy, W. Hayes, Physica B 155 (1989) 362.
[2] R. von Helmot, J. Wecker, B. Holzapfel, L. Schultz, K. Samwer, Phys. Rev. Lett. 71 (1993) 2331.
[3] S. Jin, T.H. Tiefel, M. McCormck, R.A. Fastnacht, R.L. Ramesh, H. Chen, Science 64 (1994) 413.
[4] M. Jaime, P. Lin, S.H. Chun, M.B. Salamon, P. Dorsey, M. Rubinstein, Phys. Rev. B 60 (1999) 1028.
[5] R. Laiho, K.G. Lisunov, E. Lähderanta, P.A. Petrenko, J. Salminen, V.N. Stamov, V.S. Zakhvalinskii, J. Phys.: Condens. Matter 12 (2000) 5751.
[6] R. Laiho, E. Lähderanta, J. Salminen, K.G. Lisunov, V.S. Zakhvalinskii, Phys. Rev. B 63 (2001) 094405.
[7] C.H. Chen, S.-W. Cheong, Phys. Rev. Lett. 81 (1998) 5612; S. Yunoki, A. Moreo, E. Dagotto, Phys. Rev. Lett. 81 (1998) 5612.
[8] G. Papavassiliou, M. Fardis, M. Belesi, T.G. Maris, G. Kallias, M. Pissas, D. Niarchos, C. Dimitropolus, J. Dolinsek, Phys. Rev. Lett. 84 (2000) 761.
[9] R.D. Shannon, Acta Crystallogr., Sect. A: Cryst. Phys., Diffr., Theor. Gen. Crystallogr. 32 (1976) 751.
[10] G.H. Rao, J.R. Sun, A. Kattwinkel, L. Haupt, K. Bärner, E. Schmitt, E. Gmelin, Physica B 269 (1999) 379.
[11] M.P. Simopoulos, G. Kallias, E. Devlin, N. Moutis, I. Panagiotopoulus, D. Niarchos, C. Christides, R. Sonntag, Phys. Rev. B 59 (2) (1999) 1263.
[12] I.V. Medvedeva, K. Bärner, G.H. Rao, N. Hamad, Yu.S. Bersenev, J.R. Sun, Physica B 292 (2000) 250.
[13] R. Laiho, K.G. Lisunov, E. Lähderanta, J. Salminen, V.S. Zakhvalinskii, J. Magn. Magn. Mater. 250 (2002) 267.
[14] Q. Huang, Z.W. Li, J. Li, C.K. Ong, J. Appl. Phys. 89 (11) (2001) 7410.
[15] S.L. Young, Y.C. Chen, H.Z. Chen, L. Horng, J.F. Hsueh, J. Appl. Phys. 91 (10) (2002) 8915.
[16] J. Gutierrez, A. Peña, J.M. Barandiarán, J.L. Pizarro, T. Hernández, L. Lezama, M. Insausti, T. Rojo, Phys. Rev. B 61 (13) (2000) 9028.
[17] J. Takeuchi, S. Hirahara, T.P. Dhakal, K. Miyoshi, K. Fujiwara, J. Magn. Magn. Mater. 226–230 (2001) 884.
[18] Y.L. Chang, Q. Huang, C.K. Ong, J. Appl. Phys 91 (2) (2002) 789.
[19] J. Takeuchi, A. Uemura, K. Miyoshi, K. Fujiwara, Physica B 281 & 282 (2000) 489.
[20] J.-W. Feng, C. Ye, H.-P. Hwang, Phys. Rev. B 61 (2000) 12271.
[21] H.M. Rietveld, J. Appl. Crystallogr. 2 (1969) 65.
[22] J. Rodriguez-Carvajal, Physica B 192 (1993) 55.
[23] J. Baldinozzi, J.F. Berar, J. Appl. Crystallogr. 26 (1993) 128.
[24] E. Suard, F. Fauth, C. Martin, A. Maignan, F. Millange, L. Keller, J. Magn. Magn. Mater. 264 (2003) 221.
[25] M. Tseggai, R. Mathieu, P. Nordblad, R. Tellgren, L.V. Bau, D.N.H. Nam, N.X. Phuc, N.V. Khiem, G. André, F. Bourée, J. Solid State Chem. 177 (2004) 966.
[26] J.J. Blanco, L. Lezama, M. Insausti, J. Gutierrez, J.M. Barandiarán, T. Rojo, Chem. Mater. 11 (1999) 3464.
[27] M.M. Xavier, F.A.O. Cabral, J.H. de Araújo, C. Chesman, T. Dumelow, Phys. Rev. B 63 (2000) 12408.
[28] Y.L. Chang, Q. Huang, K. Ong, J. Appl. Phys. 91 (2002) 789.
[29] S.L. Young, H.Z. Cheng, L. Horng, J.B. Shi, Y.C. Chen, Jpn. J. Appl. Phys. 40 (2001) 4878.
[30] S.M. Yusuf, M. Sahana, M.S. Hegde, K. Dörr, K.-H. Müller, Phys. Rev. B 62 (2) (2000) 1118.
[31] T.P. Dhakal, K. Miyoshi, K. Fujiwara, J. Takeuchi, J. Magn. Magn. Mater. 226–230 (2001) 824.
[32] J. Park, M.S. Kim, J.-G. Park, I.P. Swainson, H.-C. Ri, H.J. Lee, K.H. Kim, T.W. Noh, S.-W. Cheong, C. Lee, J. Korean Phys. Soc. 36 (6) (2000) 412.
[33] D.N.H. Nam, R. Mathieu, P. Nordblad, N.V. Khiem, N.X. Phuc, Phys. Rev. B 62 (2000) 1027.